Journal of the European Ceramic Society **19** (1999) 217–226

PII: S0955-2219(98)00192-7
0955-2219/98/$—see front matter

Effect of Long-term Oxidation on Creep and Failure of Si_3N_4 and Si_3N_4/SiC Nanocomposites

P. Rendtel,[a]* A. Rendtel,[a†] H. Hübner,[a] H. Klemm[b] and M. Herrmann[b]

[a]TU Hamburg-Harburg, Materials Physics Group, D-21071 Hamburg, Germany
[b]Fraunhofer-Institute for Ceramic Technologies and Sintered Materials (IKTS), D-01277 Dresden, Germany

(Received 25 February 1998; revised version received 24 July 1998; accepted 31 July 1998)

Abstract

The high-temperature mechanical behaviour of an Si_3N_4/SiC nanocomposite and its monolithic Si_3N_4 reference material was studied after long-term oxidation treatments intended to simulate future operating conditions in a severe environment. Creep and failure at elevated temperature were significantly affected, in the direction of increased brittleness. The transition stress between the ductile range present at low stresses and the brittle range existing at high stresses was shifted to distinctly lower values. The creep resistance in the low-stress range was increased by the oxidation treatment. The failure time under a given stress was drastically reduced; this was attributed to an increased sensitivity to subcritical crack growth. The failure stress for a given failure time was decreased by about half. The phenomena are explained in terms of a purification of the intergranular phase and by the formation of surface defects and of a uniformly distributed pore population. © *1998 Elsevier Science Limited. All rights reserved*

Keywords: Si_3N_4, composites, oxidation, creep behaviour, lifetime.

1 Introduction

Silicon nitride ceramics are candidate materials for structural parts in high-temperature energy conversion systems such as ceramic gas turbines or diesel engines. For these applications, oxidation-resistant materials of high mechanical strength and extremely low creep rates are needed. Under the operating conditions of up to 300 MPa at 1400°C in an oxidizing environment, structural components should exhibit a creep strain of at most 1% during a projected lifetime of 10 000 h.[1]

A large advance towards creep-resistant silicon nitride-based ceramics was achieved by developing Si_3N_4/SiC nanocomposites. The concept of ceramic nanocomposites was originally presented by Niihara.[2] In the case of Si_3N_4-based nanocomposites, a submicron-sized SiC dispersion is embedded in a submicron-sized silicon nitride matrix. The globular SiC particles are located both within Si_3N_4 grains and at Si_3N_4 grain boundaries. It has only been shown by Niihara *et al*. that the addition of the SiC dispersion resulted in considerable improvements in strength and fracture toughness at room temperature.[2,3] and in a marked increase in the hot strength and the creep resistance.[4,5] Strength data close to 1000 MPa at room temperature were measured by the present authors[6] and no variation with SiC-content or improvement could be found. The retained strength at 1400°C was found to lie between 80 and 100% of the room temperature strength.[7] Creep rates as low as $1 \times 10^{-9}\,s^{-1}$ at 1400°C and 300 MPa were reported for an Si_3N_4/SiC nanocomposite material containing 15 vol% SiC,[7,8] and this material survived a 687 h test without failure under the same conditions.[8] A summary of high-temperature strength and creep data of Si_3N_4/SiC nanocomposites as well as of possible strengthening and hardening mechanisms of the SiC particle dispersion has recently been published.[7] Chemical, direct mechanical, and microstructural interactions were suggested to be responsible for the observed hardening effects.

Knowledge about the creep performance of Si_3N_4 materials after long-term oxidation is sketchy. Previous investigations of monolithic Si_3N_4 have shown that the observed oxidation-induced changes in the thermomechanical properties are the result of microstructural changes, which can have both a beneficial and a detrimental influence.[9–11]

*To whom correspondence should be addressed.
†Now at GKSS Forschungszentrum Geesthacht GmbH, Institute for Materials Reseach, D-21502 Geesthacht, Germany.

Only very few systematic investigations of the creep behaviour of oxidized materials have been reported. It was found[12] that the high-temperature strength of Si_3N_4 was improved by an oxidation treatment whereas the room-temperature strength was much less influenced. The question still remains to be answered, however, whether the observed strength improvement was indeed caused by oxidation effects or merely by the thermal treatment. Other authors reported that a heat treatment made *in the absence* of oxygen also caused a marked decrease in the creep rate of Si_3N_4/SiC composites at 1300°C.[13] The finding was explained by the devitrification of the intergranular glass phase.

Different types of oxidation effects on the microstructure of Si_3N_4 or Si_3N_4/SiC materials are discussed in the literature.[12,14,15] According to these references, the oxidation process involves a series of complex steps. The oxidation of yttria doped Si_3N_4 or SiC starts with the formation of an amorphous SiO_2 layer on the surface. Due to the chemical gradient between the SiO_2 on the surface and the grain boundary phase in the bulk material, yttrium ions diffuse to the surface and start forming an yttrium silicate ($Y_2Si_2O_7$) layer above the silica-rich layer. Likewise, impurities are assumed to diffuse from the intergranular phase in the bulk to the silica-rich layer. Thus, beneath the outermost film formed of yttrium silicate a layer containing amorphous silica as well as cristobalite is found. Below this two-layer package, a third layer is built up that consists of the original Si_3N_4 containing a certain amount of silicon oxinitride, Si_2N_2O. All these oxidation reactions occur with a volume increase.

It was the aim of this study to investigate the effect of a long-term oxidation on the creep properties and the high-temperature failure time of Si_3N_4/SiC nanocomposites and a monolithic Si_3N_4 material of the same matrix composition. For this purpose, samples were oxidized in air at 1500°C for 1000 h prior to creep testing. Creep and failure-time data were determined experimentally and compared with those of as-fabricated materials. The oxidation treatment caused a distinct hardening and an increase in brittleness in both the monolithic and composite material grades. The reasons for these phenomena are discussed.

2 Experimental Procedure

The starting materials for specimen fabrication were a high purity α-Si_3N_4 powder (E10, Ube Industries Ltd., Japan) and a SiCN powder containing 80 wt% SiC that was prepared by a plasma-spray technique.[16] An amount of 10 wt% Y_2O_3 was added as a densification aid. Disks were produced by conventional hot-pressing at 1840°C. The details of the fabrication process have been published elsewhere.[6]

Two different materials were fabricated: a nanocomposite containing 10 vol% of SiC (designated 10YH10SCp), and a monolithic silicon nitride material made for comparison, which was intended to have exactly the same matrix composition as the nanocomposite (designated 10YH). The matrix grain size of the 10YH material was about 0·7 μm and of the 10YH10SCp material about 0·4 μm. The SiC particle size was about 0·2 μm. Both materials were tested in their as-fabricated state and after an oxidation heat treatment of 1000 h at 1500°C in air (designated 10YH10SCp-ox and 10YH-ox), giving a total of four different materials. They are summarized in Table 1. The oxidized specimens were creep-tested in the as-oxidized state, that is to say the surface scales formed during the pre-oxidation treatment were not removed prior to testing. This procedure was thought to simulate more closely future operating conditions.

Creep tests were performed in four-point bending using inner and outer spans of 20 and 40 mm, respectively. The measurements were carried out in a dead-weight creep machine in air at temperatures ranging from 1400 to 1600°C and in a range of outer fibre stresses between 70 and 600 MPa. During the creep test, the sample deflection was recorded continuously. The strain $\dot{\varepsilon}$ was taken as the outer fibre strain and calculated by the method of Hollenberg *et al.*[17] The creep rate, $\dot{\varepsilon}$ was calculated from the slope of the ε versus time curve. The accuracy of the strain measurement permitted the determination of the creep rate down to a level of $2 \times 10^{-9}\,s^{-1}$.

The steady-state creep rate $\dot{\varepsilon}_s$, of ceramics can be described by the Norton equation:[18]

$$\dot{\varepsilon}_s = A \cdot \sigma^n \cdot \frac{1}{d^m} \cdot \exp\left(-\frac{Q_c}{RT}\right) \qquad (1)$$

where A is a constant, which depends on the respective material and on its microstructure, σ is the stress, n is the stress exponent, d is the grain

Table 1. Materials investigated and creep parameters measured

Material	*SiC content (wt%)*	*Oxidation treatment*	Q_c *(kJ mol^{-1})*	n	σ_t, *(MPa)*	n*	*N*
10YH	0	None	1005	1·3	460	33	89
10YH-ox	0	1500°C/1000 h	1120	2·0	170	27	38
10YH10SCp	10	None	1290	2·2	505	40	82
10YH10SCp-ox	10	1500°C/1000 h	1585	1·6	280	30	32

size, m is the grain size exponent, Q_c is the activation energy for creep, and T and R have their usual meaning. To determine n and Q_c, stress and temperature change tests were carried out. In the temperature change tests, one sample of each grade was measured at temperatures between 1450 and 1600°C and a stress of 100 MPa. The temperature was changed stepwise after a stationary creep rate was reached. In the same way stress change tests were carried out at stresses between 70 and 300 MPa at a temperature of 1475°C. To compare the creep data generated at 1475°C with the failure time experiments measured at 1400°C, the former were normalized to 1400°C by means of eqn (1), taking the activation energy for creep of Table 1 of the respective material. The higher temperature of 1475°C chosen for the stress change tests was necessary because the creep rates at low applied stresses turned out to be very low.

To determine the failure time, t_f, samples were tested at 1400°C in bending until failure occurred. In these tests, the minimum creep rate, $\dot{\varepsilon}_{min}$ and the failure strain ε_f, were taken at t_f. To evaluate ε_f, the elastic strain was subtracted.

3 Results

3.1 Creep testing

3.1.1 Temperature change tests

A typical creep curve (ε-versus-t) of a temperature change test is shown in Fig. 1. The corresponding creep rate curve ($\dot{\varepsilon}$-versus-ε) is given in Fig. 2. The creep rate curve was used to determine steady-state creep rates for the different temperatures. These creep rates were used for the further analysis. Figure 3 shows the temperature dependence of the creep rate for the four different materials in an Arrhenius plot. The curves can be described by straight lines. For temperatures below 1550°C the monolithic material was found to creep faster than the nanocomposite. The oxidation treatment resulted in a decrease of the creep rate of the monolithic Si_3N_4 over the whole temperature range. For the composite material, on the other hand, the creep rate was reduced for temperatures below 1500°C only. At the lower end of the temperature range, the reduction in creep-rate was quite pronounced, reaching a factor of 3 to 4 in both the monolithic and the composite material grades.

Activation energy data determined from the slope of the lines of Fig. 3 are summarized in Table 1. For all materials the activation energies for creep were very high, between 1000 and nearly 1600 kJ mol^{-1}. The highest value was obtained for the pre-oxidized nanocomposite. The activation energy for creep of the monolithic material was significantly lower than that of the nanocomposite.

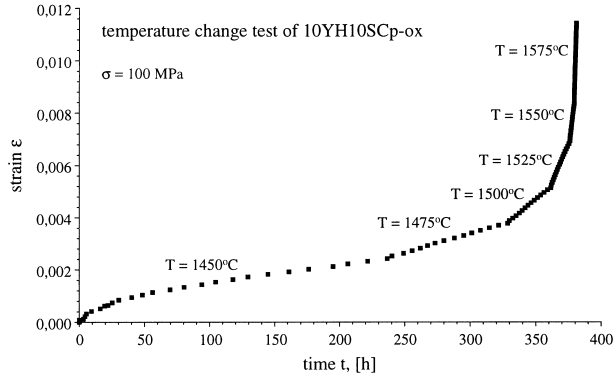

Fig. 1. Typical creep curve ε-versus-t of a temperature change test.

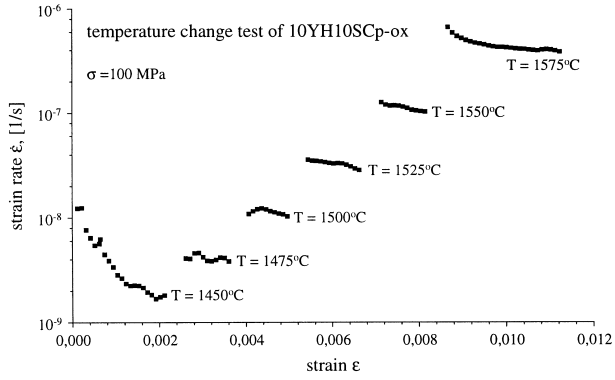

Fig. 2. Typical creep rate curve $\dot{\varepsilon}$-versus-ε of a temperature change test.

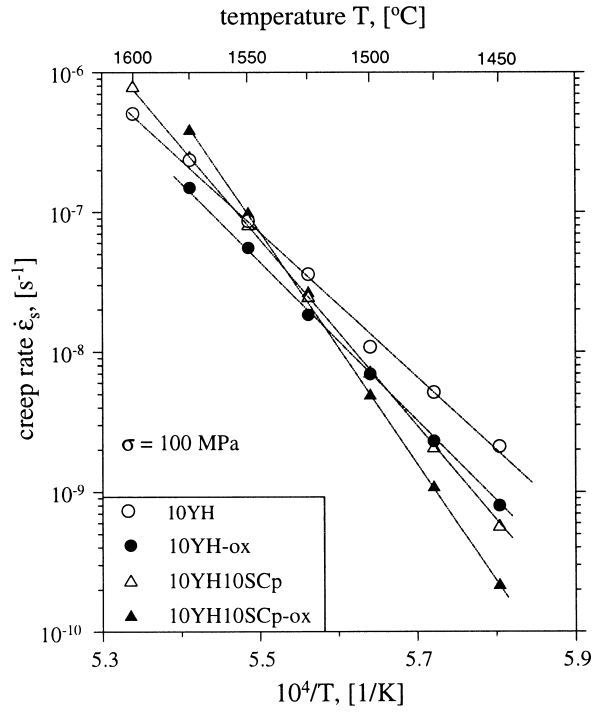

Fig. 3. Effect of temperature and oxidation treatment on the steady-state creep rate, $\dot{\varepsilon}_s$ of monolithic Si_3N_4 and of Si_3N_4/SiC nanocomposites.

After the oxidation treatment the activation energy for creep increased in both types of materials. For the composite, the increase of about 23% was much greater than for the monolithic material.

3.1.2 Stress change tests

Similar to Figs 1 and 2 typical creep curves and creep rate versus strain curves of a stress change test are shown in Figs 4 and 5, respectively. The creep rate curves like the one presented in Fig. 5 were used to calculate creep rates for the different stresses at a constant strain of $\varepsilon = 0{\cdot}008$. The stress dependence of the creep rate at 1475°C of the four materials studied is shown in Fig. 6. For a further analysis the creep rates determined at 1475°C were converted to 1400°C using eqn (1). These converted creep rates are plotted together with the minimum creep rates obtained at 1400°C in the time-to-failure tests in Fig. 7.

Two ranges of different stress dependence were observed. At low and intermediate stresses, the effect of stress on the creep rate was found to be small, and stationary creep rates were obtained. The data points could be approximated by straight lines. From the slope of these lines the stress exponent n was calculated and was found to lie between 1·3 and 2·2 (Table 1). The nanocomposite showed lower creep rates than the monolithic Si_3N_4. The oxidation treatment caused a decrease of the creep rate in both materials. Test durations of up to 500 h and strains exceeding 1% were achieved. The creep behaviour in the low-stress range of Fig. 7 can be characterized by a homogeneous bulk deformation of the test piece and a pronounced ductility at very low creep rates, and by a long failure time.

Above a certain stress, however, the creep behaviour changed drastically. The samples were

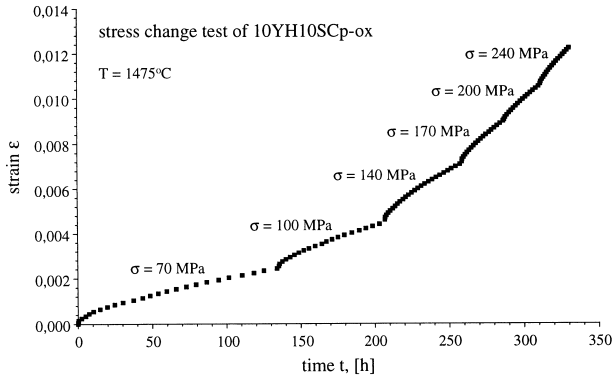

Fig. 4. Typical creep curve ε-versus-t of a stress change test.

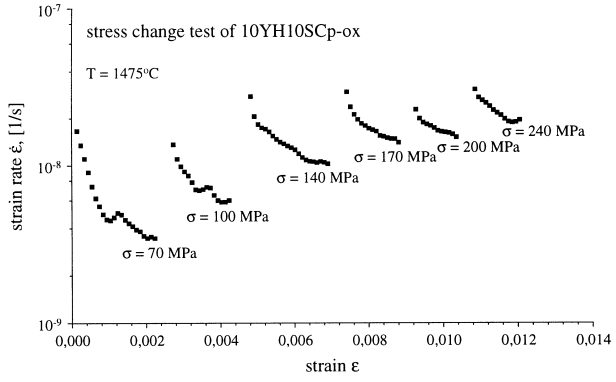

Fig. 5. Typical creep rate curve $\dot{\varepsilon}$-versus-ε of a stress change test.

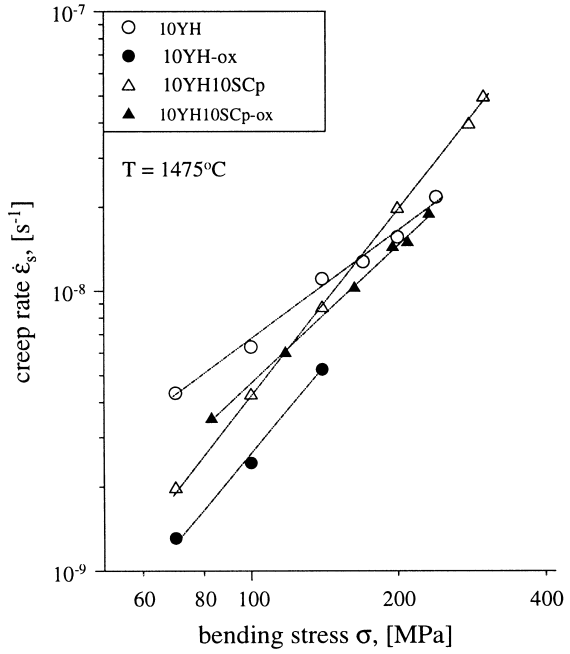

Fig. 6. Effect of stress and oxidation treatment on the steady-state creep rate, $\dot{\varepsilon}_s$, at 1475°C (data as measured).

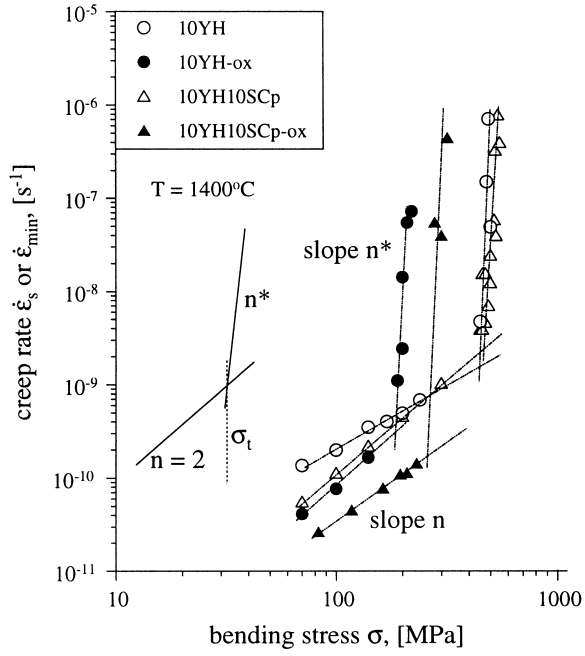

Fig. 7. Effect of stress and oxidation treatment on the steady-state or minimum creep rate, $\dot{\varepsilon}_s$ and $\dot{\varepsilon}_{min}$, at 1400°C ($\dot{\varepsilon}_s$ data converted from 1475°C to 1400°C).

damaged by cracking and failed before reaching a steady-state creep stage. Therefore, only minimum creep rates could be determined in the high-stress regime. Figure 7 shows that the creep rate exhibited a very strong stress dependence with an apparent stress exponent n^* between 27 and 40 (Table 1). The nanocomposite grades, both as-fabricated and pre-oxidized, were found to creep slower than the monolithic reference material. As will be shown in the next subsection, the failure times became very short and decreased dramatically as the stress was only slightly increased.

The same result was found for the failure strain, ε_f, which is plotted in Fig. 8 as a function of the applied stress. It decreased rapidly with increasing stress, and at stresses typical for the high-stress regime of Fig. 7 it dropped to a level of only some 10^{-4} to 10^{-3}. Two data points of the 10YH10SCp material, obtained in the low-stress regime, are included in Fig. 8 for comparison (the two triangles marked by circles). They represent creep strains attained at a test duration of 337 and 498 h when the tests were stopped intentionally. The two data points demonstrate how strongly the ductility increased as the stress was reduced only slightly, indicating a very sharp transition between the regimes of high and low stresses.

Figure 8 also shows two specific oxidation-induced features. Failure of pre-oxidized materials occurred at a greatly reduced stress level; also, the pre-oxidized materials, in contrast to the two as-fabricated grades, did not exhibit an increase in failure strain at decreasing stress. These observations are seen as an indication that the oxidation treatment resulted in a widely reduced ductility at elevated temperatures.

The two ranges of different stress response were observed for each of the four materials studied. They can readily be recognized in Fig. 7 by their different slopes. The different stress dependencies give rise to an intersection of the $\dot{\varepsilon}$-versus-σ curves at a well-defined stress, called the transition stress, σ_t. The transition stress was high and nearly the same for the as-fabricated monolithic and composite materials (460 and 505 MPa, respectively). The oxidation treatment caused σ_t to decrease markedly from 460 to 170 MPa in the monolithic Si_3N_4, whereas the decrease in the nanocomposite was less pronounced (from 505 to 280 MPa). Transition stress data are listed in Table 1. Apparently, pre-oxidation resulted in an extension of the range of brittle behaviour to lower stresses.

The oxidation-induced increase in brittleness can be further illustrated by comparing the shape of the creep curves recorded before and after the oxidation treatment. Figure 9 shows creep curves for the 10YH10SCp nanocomposite in its as-fabricated and pre-oxidized state. The curves were determined under the same conditions of stress (300 MPa) and temperature (1400°C). In the case of the as-fabricated material, the applied stress was smaller than the transition stress ($\sigma_t = 505$ MPa), whereas for the pre-oxidized material it exceeded the transition stress ($\sigma_t = 280$ MPa). Thus, the as-fabricated specimen was creep-tested in its low-stress regime and the pre-oxidized one in its high-stress regime. Up to a test duration of about 4 h, the creep behaviour of both materials was very similar and the creep rates did not differ much from each other. The as-fabricated grade (10YH10SCp) continued creeping up to a total time of 400 h when the creep test was stopped intentionally (note the change in the time scale in Fig. 9 after a test time of 5 h). The pre-oxidized grade (10YH10SCp-ox), however, suddenly exhibited an abrupt strain increase due to crack formation, and underwent rupture shortly afterwards, reaching a test duration of just over 4 h. This is a reduction in lifetime by at least a factor of 100 as compared with the as-fabricated grade.

3.1.3 Failure time

In Fig. 10 the stress dependence of the failure time, t_f, is shown at 1400°C in a log–log plot. It will be shown in the discussion that failure models exist that predict a linear dependence between log σ_f and log t_f with a slope equal to $-1/N$ where N is the

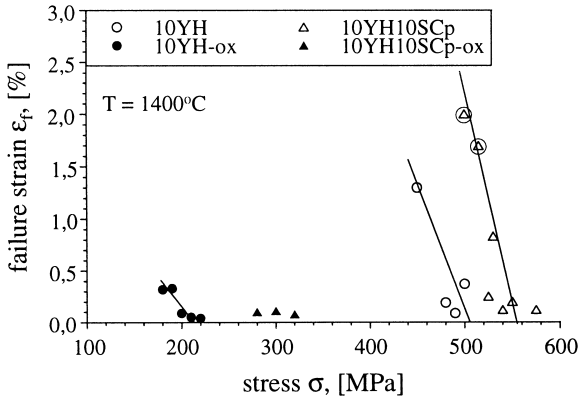

Fig. 8. Effect of stress and oxidation treatment on the failure strain, ε_f, at 1400°C.

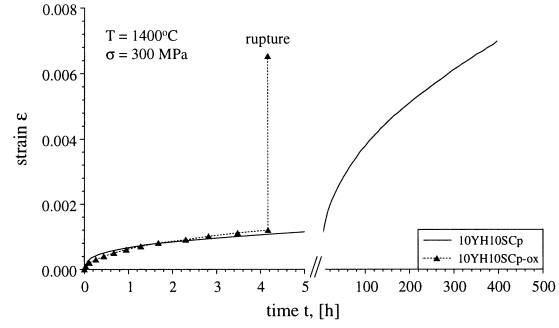

Fig. 9. Creep curves of 10YH10SCp nanocomposite in the as-fabricated and pre-oxidized state.

characteristic exponent of the corresponding model. The data points of Fig. 10 were approximated by straight lines, and exponents N calculated from the slopes of these lines; these exponents are listed in Table 1. The high numerical values of N are indicative of a failure mechanism controlled by subcritical crack growth. Thus, N can be taken as the crack-growth exponent of the respective material.

Both the monolithic and the composite material were weakened drastically by the oxidation treatment, the former even more than the latter. As can easily be seen from Fig. 10, two important changes in the time-to-failure behaviour were observed. The stress level at a given failure time was reduced to about one half, and the crack-growth exponent decreased considerably. Both features are indications that crack expansion is promoted in the oxidized materials. It should also be pointed out that, after oxidation, the failure stress for a given failure time was distinctly larger in the nanocomposites than in the monolithic Si_3N_4. This finding demonstrates that the nanocomposite material exhibited a higher resistance to oxidation-induced damage than the monolithic standard material.

The data points marked by arrows in Fig. 10 indicate specimens that did not fail during the creep tests. These data points are located at the lower bound of the stress range employed for failure-time testing and are indicating that they are close to the transition stress defined above. As further evidence of the abrupt change in mechanical response, transition stress data from Table 1 are shown in Fig. 10 as horizontal dashed lines. It can be seen that the stress level at which the first test survivors were observed agrees reasonably well with the transition stress of Fig. 7, obtained by a completely different test technique.

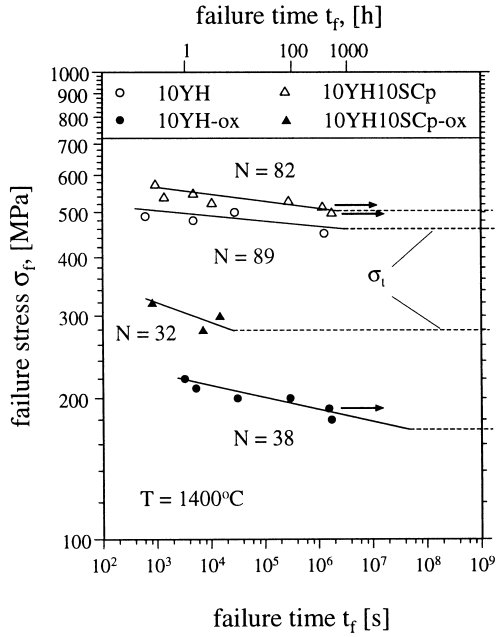

Fig. 10. Effect of stress and oxidation treatment on the failure time, t_f, at 1400°C.

3.2 Micrographic observations

To detect possible influences of the oxidation process on a microscopic scale, the morphology of the oxide layers and the microstructure of the bulk material were examined. In Fig. 11(a) and (b) polished cross sections of the pre-oxidized monolithic Si_3N_4 and of the Si_3N_4/SiC nanocomposite are shown. The appearance of the oxide scale of both materials was similar. Three different layers could be distinguished. The outermost layer (1) consisted of $Y_2Si_2O_7$ crystals occasionally containing small cavities. The subsequent layer (2) was more porous and contained silica portions. Finally, a third layer (3) containing Si_2N_2O embedded in the bulk material was identified. These findings agree well with results reported by other

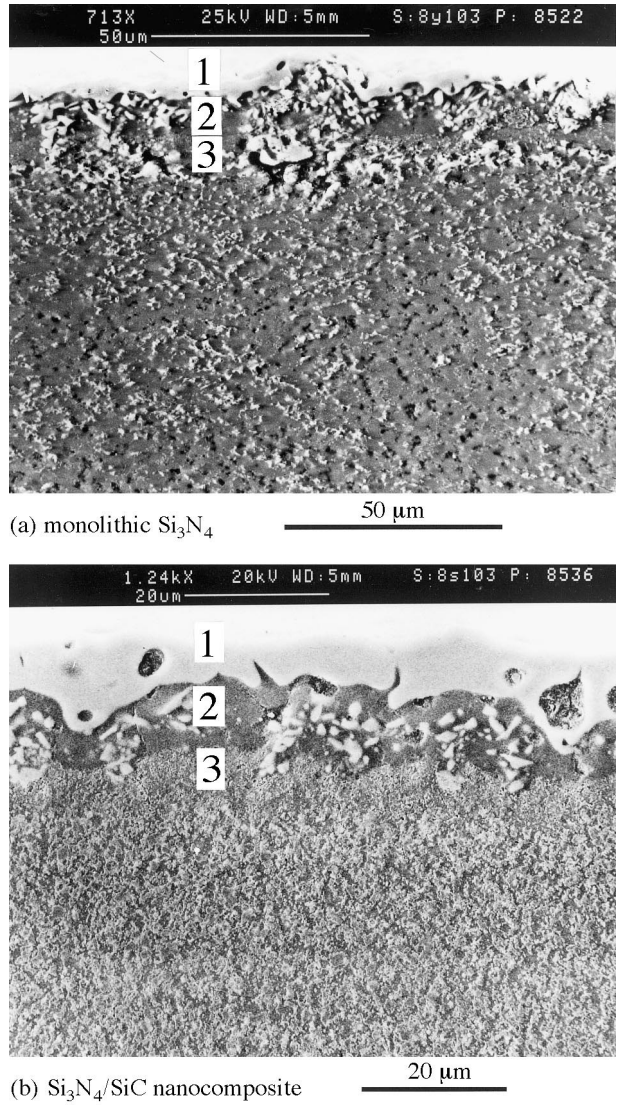

Fig. 11. SEM micrographs of oxidation layers formed on (a) monolithic Si_3N_4, and (b) Si_3N_4/SiC nanocomposite.

authors.[12,14,15] The Si_2N_2O-rich layer was found to be thicker and to contain more Si_2N_2O in the composite than in the monolithic material. As a further result of the oxidation process, surface pits of a diameter between 15 and 50 μm were found. Their size was smaller in the nanocomposite than in the Si_3N_4 standard material.

Within the whole bulk material pores were formed by the oxidation treatment (dark dots in the micrographs of Fig. 11(a) and (b)). The pore size was in the range between 0·2 and 1 μm. The pore fraction was determined by image analysis and plotted in Fig. 12 as a function of the square root of the oxidation time, t_{ox}. A parabolic time law was found. In the monolithic reference material the pore fraction after an oxidation time of 1000 h was 4·7% which seems to be a surprisingly large number. It was about seven times larger than in the nanocomposite.

4 Discussion

The modifications of the creep properties and the failure time that were found to be caused by the long-term oxidation treatment will be discussed in the following subsections. However, the occurrence of the two stress regimes themselves will not be explicitely addressed, since they were already observed in the as-fabricated materials.[8]

4.1 Creep behaviour

Oxidation-induced changes in the properties of the materials can be summarized by the following three main results of the present investigations.

1. In the low-stress regime, i.e. at $\sigma < \sigma_t$, the creep resistance was enhanced (Fig. 7) and the activation energy for creep was increased (Fig. 3 and Table 1). The stress exponent, however, was not altered.

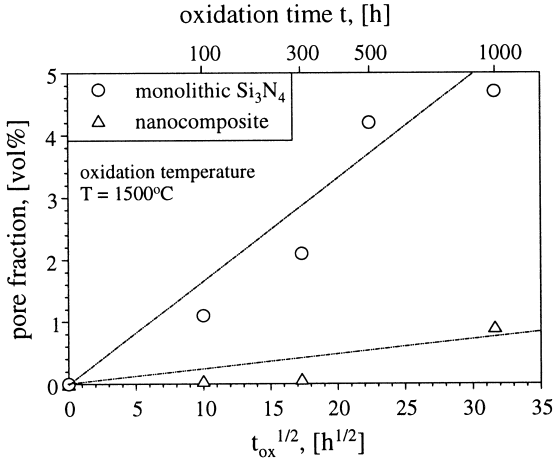

Fig. 12. Effect of oxidation time on pore formation at 1500°C.

2. In the high-stress regime, $\sigma > \sigma_t$, the failure strain, ε_f, was reduced to nearly zero, but the stress exponent, n^*, remained essentially unchanged (Table 1).
3. The upper bound of the low-stress regime, i.e. the transition stress σ_t, was reduced (Fig. 7).

One of the principal phenomena observed in oxidation studies of silicon nitride materials is the outward diffusion of impurities and additive cations.[12,19,20] These elements are attracted by the freshly formed, pure surface layers and diluted over a larger volume. The outward diffusion results in a 'cleaning' of the grain-boundary phase and, consequently, in an increase in its viscosity. On the other hand, it has been demonstrated that the intentional contamination of a clean intergranular amorphous phase in Si_3N_4 by small amounts of a fluorine dopant was able to reduce the viscosity of the grain-boundary film.[21] Thus, the observed increase in the creep resistance at $\sigma < \sigma_t$ is thought to be caused by the reduction of the impurity concentration in the amorphous grain-boundary phase. Furthermore, the degree of crystallization of the grain-boundary phase may also have been changed by the long-term thermal treatment during oxidation, as was reported previously by other authors.[13] However, no change in the grain-boundary phase composition in the bulk material could be detected by X-ray diffraction analysis.

The stress exponents listed in Table 1 cover a range from 1·3 to 2·2. This range is typical for stress exponent data found in creep tests performed in bending. Furthermore, they exhibit no unequivocal alteration due to the oxidation treatment. This indicates that the basic creep mechanism acting in the low-stress regime was not affected by the oxidation treatment. Moreover, the stress exponents are distinctly different from those determined for other creep mechanisms like dislocation creep. Dilatational creep has been proposed to be the deformation mechanism in monolithic Si_3N_4 under tensile loading.[22] It has also been suggested to control the creep of Si_3N_4/SiC nanocomposites.[7] The pronounced increase in the activation energy for creep cannot be explained at present.

The decrease in the transition stress and in the failure strain axe evidence of an expansion of the range of predominantly brittle behaviour. In ceramic materials, brittle behaviour is usually encountered at low temperatures, high stresses, high deformation rates, and with a coarse grain size.[23] Apparently, chemical and microstructural modifications were initiated during the oxidation treatment that contributed to an extension of the brittle regime to lower stresses. The details of such modifications, which could be able to impede the

deformation process, are not known. In any case, grain growth as a mechanism to reduce creep deformation can be excluded for the oxidation treatment at 1500°C. For similar treated silicon nitrides no unambiguously coarsening of the microstructure was observed.[24] A distinct grain growth by a maximum factor of 5 was only detected after a heat treatment at 1900°C.[25] Furthermore, the grain size effect on the creep rate is relatively small, since the grain size exponent is 1 for silicon nitride.[25] The enhancement of brittleness coincides well with the observations on the failure behaviour discussed in the following subsection.

4.2 Failure time

The principal features of the failure behaviour can be summarized as follows.

1. Failure was observed to occur in the high-stress regime of Fig. 7 where brittle behaviour prevailed. From a plot of failure time versus stress (Fig. 10), very large exponents N were obtained that were substantially smaller in the oxidized materials. The strain at failure was very small.
2. After oxidation the stress level sustained by both the nanocomposite and the monolithic Si_3N_4 to yield a given failure time was only about half that of the as-fabricated materials.

High-temperature failure of ceramics is controlled either by subcritical crack growth or by the accumulation of creep damage. In the former case, the time to failure under static loading conditions is given by the relationship[26]

$$t_f = B \cdot \frac{S_I^{N-2}}{\sigma_f^N} \tag{2}$$

where S_I is the inert strength of the material (i.e. the strength in the absence of subcritical crack growth), σ_f is the failure stress, N is the crack growth exponent, and B is an abbreviation for $B = 2/\{AY^2(N-2)K_{Ic}^N - 2\}$ with Y the stress intensity calibration of fracture mechanics and K_{Ic} the fracture toughness. Failure controlled by creep damage, on the other hand, is described by the Monkman–Grant relationship[27]

$$\dot{\varepsilon}_s \cdot t_f = \text{const} \tag{3}$$

Substituting $\dot{\varepsilon}_s$ from eqn (1) into eqn (3) gives

$$t_f = \frac{\text{const}}{\sigma_f^n} \tag{4}$$

with n the stress exponent of the Norton equation.

Equations (2) and (4) predict the slope of a plot like that of Fig. 10 to be equal to $-1/N$ or $-1/n$, respectively. From the values obtained from Fig. 10 ($32 < N < 89$) as well as from the stress exponent of the creep rate ($n \approx 2$) it is concluded that, in the materials of the present study, the failure time is controlled by the growth of individual cracks rather than by creep damage accumulation, and that failure is initiated when the critical failure size is reached. The predominance of brittle phenomena at high stresses is further substantiated by the very small failure strains.

The fall in the crack-growth exponents from values around 80 *before* oxidation to values between 30 and 40 *after* oxidation is an indication that the proneness to subcritical crack growth was increased by the oxidation treatment. The smaller the value of the crack-growth exponent in a ceramic, the more pronounced is the occurrence of subcritical crack propagation before the onset of catastrophic failure. The improved resistance of Si_3N_4-based nanocomposites to high-temperature crack growth has been explained by the increased grain-boundary strength, which is thought to be caused by the observed direct bonding at the SiC/Si_3N_4 interface.[2] Inverting this explanation, it is concluded that the *acceleration* of crack propagation may be due to a weakening of the grain-boundary strength. This concept, however, does not agree with the idea of oxidation-induced purification of the intergranular phase, which was proposed above to explain the increased creep-resistance of pre-oxidized specimens.

Another explanation of accelerated crack propagation could be the pore formation observed throughout the bulk of the oxidized materials. The diameter of these pores was found to lie between 0·2 and 1 μm. If we assume a mean pore size of 0·5 μm, and if we assume further, for a porosity of 5%, the pores to be packed in a simple cubic array, the mean pore distance is 3 μm. Compared with the grain size of the monolithic Si_3N_4 (0·7 μm) and of the nanocomposite (0·4 μm), this figure means that a crack propagating along the Si_3N_4 grain boundaries will come upon a pore after separating about 4 grains in the monolithic Si_3N_4 and about 7 grains in the nanocomposite. These pre-cracked sites along the crack path are certain to contribute to facilitating the crack advancement.

The mechanism of pore formation during oxidation is not fully understood. Several possibilities have been discussed.[12] Reactions leading to the formation of the oxidation products SiO_2, $Y_2Si_2O_7$ and Si_2N_2O are related to a volume increase. It was suggested that, due to this volume increase, a compressive stress is built up in the surface layer and a tensile stress in the bulk. Recent investigations

showed that tensile creep of Si_3N_4 resulted in extensive cavity formation.[22] There was a nearly 1:1 relationship between creep strain and porosity, that is to say 1% deformation was accompanied by 1% pore formation. Applied to our results this finding means that the porosity found in the present study must have been formed by the operation of at least one further mechanism. A possible contribution may be the outward diffusion of yttrium ions.

Finally, the reduced failure stress levels of the 10YH-ox and 10YH10SCp-ox materials, shown in Fig. 10, are analysed. Since high-temperature failure of the present materials is controlled by crack propagation, eqn (2) should apply. It predicts a failure stress for a given failure time that scales with the inert strength, S_I. Room temperature strength data measured before and after oxidation revealed a pronounced strength drop. In the monolithic Si_3N_4, the reduction was from 1000 to 470 MPa, and in the nanocomposite from 955 to 790 MPa. The corresponding flaw sizes (for $K_{Ic} = 8\,\text{MPa}\,\text{m}^{1/2}$ according to Ref. 6) increased from 16 to 72 μm (mono) and from 18 to 25 μm (nano). The relative amount of these strength reductions agrees reasonably well with those obtained from Fig. 10 at short failure times and high loadings when the amount of crack propagation is still small. Moreover, the increased flaw sizes coincide with the size range of oxidation-induced surface pits observed microscopically. The smaller surface damage found in the nanocomposite material may account for the higher failure stress of the 10YH10SCp-ox material. This finding is in agreement with other studies[20,28] where it was found that the presence of Si_2N_2O in Si_3N_4 materials reduced the oxidation damage (cracks or pores) in the surface region. It is concluded, therefore, that the reduced failure stresses of Fig. 10 are caused by the surface defects formed in the oxide scale.

5 Conclusions

The present study has shown that long-term oxidation treatments of Si_3N_4/SiC nanocomposites and of a monolithic Si_3N_4 reference material resulted in distinct changes of the high-temperature mechanical properties in the direction of enhanced brittleness. The high-stress range of mechanical response, characterized by predominantly brittle behaviour and a marked flaw sensitivity, was extended to lower stresses, while the low-stress range, where the behaviour is dominated by a homogeneous bulk deformation, a steady-state creep regime, and a plasticity of several per cent (Figs 7 and 8), is more confined. The transition stress σ_t between the two regimes was shifted to lower values. Since the service stress in an engineering application must not exceed the upper bound of the ductile regime, an important implication for safe operation is that the maximum service stress must be reduced when the material is exposed to an oxidizing environment. When this design criterion is neglected the material will be operated under conditions where the lifetime will be drastically reduced with increasing service time (Figs 9 and 10). A 10% addition of a nanosized SiC dispersion is able to increase the creep resistance in the low-stress regime and to improve the resistance to oxidation-induced damage, conferring a prolonged failure time in the high-stress regime.

Acknowledgements

The authors would like to thank the Deutsche Forschungsgemeinschaft, Bonn, for financial support (reference numbers Hu 215/7 and He 1958/3).

References

1. Pezzotti, G., Si_3N_4/SiC-platelet composites without sintering aids: a candidate for gas turbine engines. *J. Am. Ceram. Soc*., 1993, **76**, 1313–1320.
2. Niihara, K., New design concept of structural ceramics-ceramic nanocomposites. *J. Ceram. Soc. Jpn*., 1991, **99**, 9740–982.
3. Niihara, K., Hirano, T., Nakahira, A., Ojima, K., Izaki, K. and Kawakami, T., High-temperature performance of Si_3N_4-SiC composites from fine, amorphous Si-C-N powder. In *Proceedings of MRS International Meeting on Advanced Materials*, Vol. 5. Materials Research Society, Pittsburgh, 1989, pp. 107–112.
4. Niihara, K., Izaki, K. and Kawakami, T., Hot-Pressed Si_3N_4-32% SiC nanocomposite from amorphous Si-C-N powder with improved strength above 1200°C. *J. Mat. Sci. Lett*., 1990, **10**, 112–114.
5. Niihara, K., Hirano, T., Izaki, K. and Wakai, R., High temperature creep/deformation of Si_3N_4/SiC nanocomposites. *Ceram. Trans*., 1994, **42**, 207–219.
6. Herrmann, M., Schubert, C., Rendtel, A. and Hübner, H., Si_3N_4/SIC nanocomposite materials: I, Fabrication and mechanical properties at room temperature. *J. Am. Ceram. Soc*., 1998, **81**, 1095–1108.
7. Rendtel, A., Hübner, H., Herrmann, M. and Schubert, C., Si_3N_4/SiC nanocomposite materials: II, Hot strength, creep, and oxidation resistance. *J. Am. Ceram. Soc*., 1998, **81**, 1109–1120.
8. Rendtel, A. and Hübner, H., Creep behavior and lifetime of Si_3N_4/SiC nanocomposites. *Ceram. Trans*., 1996, **74**, 523–534.
9. Ogbuji, L. U. J. T. and Bryan, S. R., The SiO_2–Si_3N_4 interface, part 1: Nature of the interphase. *J. Am. Ceram. Soc*., 1995, **78**, 1272–1278.
10. Ogbuji, L. U. J. T., The SiO_2–Si_3N_4 interface, part II: O_2 permeation and oxidation reaction. *J. Am. Ceram. Soc*., 1995, **78**, 1272–1278.
11. Rho, H. S., Hecht, N. L. and Graves, G. A., The behavior of two Si_3N_4 and two SiC ceramics subject to oxidation environments. *Ceram. Eng. Sci. Proc*., 1997, **18**, 633–643.
12. Lange, F. F., Davis, B. I. and Metcalf, M. G., Strengthening of polyphase Si_3N_4 material through oxidation. *J. Mat. Sci*., 1983, **18**, 1497–1505.

13. Ramoul-Badache, K. and Lancin, M., Si_3N_4-SiC particulate composites: devitrification of the intergranular phase and its effect on creep. *J. Eur. Ceram. Soc.*, 1992, **11**, 369–379.
14. Sheldon, B. W., Silicon nitride oxidation based on oxynitride interlayers with graded stoichiometry. *J. Am. Ceram. Soc.*, 1996, **79**, 2993–2996.
15. O'Meara, C. and Sjöberg, J., Transmission electron microscopy investigation of the oxidation of hot isostatically pressed silicon nitride with and without sintering aids. *J. Am. Ceram. Soc.*, 1997, **80**, 1491–1500.
16. Zalite, L, Boden, G., Schubert, C., Lodzina, A., Plitmanis, J. and Miller, T., Sintering of fine silicon nitride powders. *Latvian Chemical Journal*, 1992, **2**, 152–159.
17. Hollenberg, G. W., Terwilliger, G. R. and Gordon, R. S., Calculation of stresses and strains in four-point bending creep tests. *J. Am. Ceram. Soc.*, 1971, **54**, 196–199.
18. Norton, F. H., The flow of ceramic bodies at elevated temperatures. *J. Am. Ceram. Soc.*, 1936, **19**, 129–314.
19. Clarke, D. R., Thermodynamic mechanism for diffusion through an intergranular phase: application to environmental reactions with nitrogen ceramics. In *Progress in Nitrogen Ceramics*, ed. F. L. Riley. Martinus Nijhoff Publishers, The Hague, 1983, pp. 421–426.
20. Klemm, H., Herrmann, M. and Schubert, C., Silicon nitride composites materials with an improved high temperature oxidation resistance. *Ceram. Eng. Sci. Proc.*, 1997, **18**, 615–623.
21. Pezzotti, G. and Ota, K., Grain-boundary sliding in fluorine-doped silicon nitride. *J. Am. Ceram. Soc.*, 1997, **80**, 599–603.
22. Luecke, W. E., Wiederhorn, S. M., Hockey, B. J., Krause Jr, R. F. and Long, G. G., Cavitation contributes substantially to tensile creep in silicon nitride. *J. Am. Ceram. Soc.*, 1995, **78**, 20855–2096.
23. Frost, H. J. and Ashby, M. F., *Deformation-Mechanism Maps*. Pergamon Press, New York, 1982.
24. Klemm, H., Herrmann, M. and Schubert, C., High Temperature Oxidation and Corrosion of Silicon-Based Nonoxide Ceramics. *International Gas Turbine and Aeroengine Congress and Exhibition*, ASME-Paper 98/GT/480, Stockholm, Sweden, 1998.
25. Acchar, W., Rendtel, A., Hübner, H. and Schubert, C., Improvements in the creep resistance of hot-pressed silicon nitride (HPSN). In *Engineering Ceramics (Third euroceramics*, **Vol. 3**), ed. P. Duran and J. F. Fernáindez, Faenza Editrice Ibérica S. L., 1993, pp. 405–410.
26. Davidge, R. W., MacLaren, J. R. and Tappin, G., Strength-probability-time (SPT) relationships in ceramics. *J. Mat. Sci.*, 1973, **8**, 1699–1705.
27. Monkman, F. C. and Grant, N. J., An empirical relationship between rupture life and minimum creep rate in creep rupture tests. *Proc. ASTM*, 1956, **56**, 593–605.
28. Klemm, H., Tangermann, K., Schubert, C. and Hermel, W., Influence of molybdenum silicide additions on high-temperature oxidation resistance of silicon nitride materials. *J. Am. Ceram. Soc.*, 1996, **79**, 2429–2435.